Proton momentum distribution and anomalous scattering intensities in a pseudo-spherical ammonium ion: a neutron Compton scattering study of $(NH_4)_2PdCl_6$ and $(NH_4)_2TeCl_6$

2009 J. Phys.: Condens. Matter 21 075502

(http://iopscience.iop.org/0953-8984/21/7/075502)

J. Phys.: Condens. Matter **21** (2009) 075502 (13pp) doi:10.1088/0953-8984/21/7/075502

Proton momentum distribution and anomalous scattering intensities in a pseudo-spherical ammonium ion: a neutron Compton scattering study of $(NH_4)_2PdCl_6$ and $(NH_4)_2TeCl_6$

M Krzystyniak[1], Z T Lalowicz[2], C A Chatzidimitriou-Dreismann[3] and M Lerch[3]

[1] Rutherford Appleton Laboratory, ISIS Facility, Chilton OX11 0QX, UK
[2] Institute of Nuclear Physics, Polish Academy of Sciences, ulica Radzikowskiego 152, 31-342 Krakow, Poland
[3] Institute of Chemistry, Technical University of Berlin, Strasse des 17. Juni 135, D-10623, Berlin, Germany

E-mail: matthew.krzystyniak@stfc.ac.uk

Received 2 December 2008
Published 23 January 2009
Online at stacks.iop.org/JPhysCM/21/075502

Abstract
Neutron Compton scattering (NCS) measurements on ammonium hexachloropalladate and hexachlorotellurate were performed at room temperature. Proton scattering intensities and momentum distributions, as measured in the NCS experiment, have been compared with results expected from the impulse approximation (IA) for both systems. The measurement shows that scattering intensity from protons is anomalous even though their momentum distribution has a second moment that agrees very well with the *ab initio* calculation for an isolated pseudo-spherical NH_4^+ ion in the ground vibrational state. Detailed data analysis shows that there is no extra (beyond the IA expected value) broadening or peak shift of proton momentum distribution due to ultra-fast kinetics of the Compton scattering process leading to anomalous scattering intensities. This is most probably due to highly symmetric local potential in the NH_4^+. Presented results have interesting implications for further theoretical work in the field.

1. Introduction

Neutron Compton scattering (NCS) is a unique method that can be applied to the investigation of proton momentum distribution reflecting protons' ultra-fast dynamics in condensed matter [1–3]. One of the phenomena discovered using the NCS method was the deficit in the scattering intensity from protons, originally measured on the unique time-of-flight (TOF) spectrometer VESUVIO at the ISIS pulsed neutron source [11]. Since then, this striking effect has been observed in liquids (water, benzene, etc) and solids (metal hydrogen systems, organic polymers, etc) (see, e.g., [11–17]). Recently this phenomenon has been confirmed by an independent method: electron Compton scattering from nuclei (ECS) [18, 19].

In the light of recent theoretical models an ultra-fast scattering process may induce changes in the proton momentum distribution. In the model proposed by Gidopoulos [34] the sub-femtosecond timescale of the NCS process, corresponding to a large energy spread of the proton wavepacket after collision, allows the proton to access excited electronic levels. This non-adiabatic excitation of electrons leads to a distortion of the shape of the neutron scattering response function with some redistribution of intensity at energies higher than the nuclear recoil energy and a slight shift of the main neutron intensity peak to lower energies [34].

In another theoretical model, Reiter and Platzman have shown that a breakdown of the Born–Oppenheimer approximation in the final state of an ultra-fast scattering

process may lead to a deficit of the scattering intensity [35]. In the theoretical model presented by these authors the final state contains a very rapidly moving proton with sufficient energy to mix the electronic states of the system. The authors predict that the contribution of the excited electronic levels to the overall NCS scattering function has the same functional form as the usual impulse approximation result, but is shifted to high energies by the difference in energies of the electronic states. The theory of Reiter and Platzman predicts a shift of the center of gravity of the proton recoil peak towards lower energies. This is necessary to compensate for the intensity shifted to high energies, since the first moment of the momentum distribution is unchanged by the corrections to the Born–Oppenheimer approximation [35].

Another interesting theoretical question that arises in the context of the ultra-fast scattering process is whether Fermi's golden rule is always true for Compton scattering. Motivated by the NCS experiments showing the anomaly of the scattering intensity of protons Mazets *et al* [36] present an example of a situation where Fermi's golden rule does not apply even if an unstable quantum system (composed of neutron, target nuclei and electrons) decays exponentially. The work of Mazets *et al* [36] aims at understanding why remarkably, and according to present-day experimental accuracy, the shortfall of scattering intensity of protons seems not to be accompanied by marked additional spectral broadening (beyond the broadening caused by the momentum width of the localized protons) of the scattering peaks. The authors analyze the possibility that coupling to the environment (electronic degrees of freedom) may change the scattering cross section (compared to that of free projectile and target particles) without causing an appreciable broadening of the scattering lineshape.

Yet another model aiming at explaining why no marked distortion of the shape of proton momentum distribution is observed in NCS experiments was proposed by Karlsson and Lovesey [37–39]. The model explains the intensity deficit without involving any participation of a third body (e.g. electrons) in the scattering process. The intensity loss is caused by destructive interference in the waves representing the scattered neutron and the recoiling particle. These interferences appear when the scattering particles are indistinguishable when seen by the neutron.

In the context of the theoretical models discussed above ammonium hexachlorometallates, $(NH_4)_2MeCl_6$ with Me = Pd, Pt, Ir, Os, Re, Se, Sn, Te and Pb, seem to be very well suited for systematic NCS studies of the scattering intensity deficit as they constitute a set of compounds with electronic properties changing in a systematic way [32, 28]. They can be ordered according to decreasing tunneling frequency (TF) of ammonium ions, which is related to the increasing potential barrier of the rotational motion [29–31, 28]. Previous measurements using the NCS technique in $(NH_4)_2PdCl_6$ and $(NH_4)_2TeCl_6$ at room temperature [32] showed that the scattering intensity of NH_4^+ protons was, in both systems, anomalous by about 20% at scattering angles approx. 60°–70°. With decreasing scattering angle the anomaly decreased almost linearly, to cease at approx. 30°. This is the second observation reported in the literature where the onset of the anomaly was observed, the first being the NCS measurement on niobium hydride [17]. The onset seems to be observed at scattering times of the order of a femtosecond where the scattering process becomes an order of magnitude slower than it is at approx. 60°–70° [1, 32]. Two further interesting observations were made in the original work on $(NH_4)_2PdCl_6$ and $(NH_4)_2TeCl_6$ [32]: (i) the dependence of the magnitude of the anomaly on the scattering angle was almost identical in both systems even though ammonium ions exhibit two entirely different electronic environments due to metal–chlorine bonding in the neighboring $MeCl_6^{2-}$ octahedra and (ii) the measured widths of proton momentum distributions are equal in both systems and independent of the scattering angle. Based on these two observations two hypotheses were put forward [32]: (i) proton dynamics of ammonium cations is decoupled from the dynamics of the sublattice of the octahedral anions $PdCl_6^{2-}$ and $TeCl_6^{2-}$, respectively, and (ii) proton–electron decoherence processes, involving the electronic cloud of the ammonium ions, are responsible for the observed dependence of the anomaly on the scattering angle [32]. Clearly, further insight into the proton momentum distribution in both systems in the context of the anomaly of the scattering intensity of protons is highly desirable.

In the bulk of the experimental NCS literature dealing with protons in condensed matter systems and molecules two lines of research have been pursued so far in their own right [3]: (i) either only the magnitude of the anomaly of the scattering intensity of protons has been investigated as a function of the scattering angle or (ii) proton momentum distributions have been measured and contrasted with theoretical predictions of single-particle dynamics without making any connection to the question of the anomaly of scattering intensities. Is the magnitude of the anomaly in any way correlated with the magnitude of the broadening of proton momentum distribution due to ultra-fast scattering kinetics, as suggested by theoretical models? Is the anomaly accompanied by any lineshape broadening at all? Are any lineshift effects due to the corrections to the Born–Oppenheimer approximation detectable under realistic conditions of an NCS measurement? To our knowledge no experimental NCS paper has ever dealt with any of these questions.

The aim of this paper is to investigate whether the previously measured anomaly of the proton scattering intensity in ammonium hexachloropalladate $(NH_4)_2PdCl_6$ and ammonium hexachlorotellurate $(NH_4)_2TeCl_6$ is accompanied by any distortions of the proton momentum distribution. The width of the proton momentum distribution is calculated from semiclassical *ab initio* analysis of vibrational, translational and rotational motion in an isolated NH_4^+ molecule in the ground vibrational state without taking into account any electronic degrees of freedom. The results of the calculation are contrasted with an advanced data reduction scheme that extracts the proton momentum distribution from measured NCS time-of-flight (TOF) spectra using the Gram–Charlier expansion [3, 4], taking into account anharmonic contributions. The results of the data reduction are found to be in very good agreement with previously published experimental results on hexachlorometallates [32] and with the result of the *ab initio*

calculation. Moreover, the scattering intensities of protons, measured previously in both hexachlorometallates [32], are compared with theoretical values expected from the IA using two novel NCS data treatment schemes: the model-free Dorner method [26, 48–50] and the center-of-peak method [27]. Both of them have been extended for the case of more than two recoil peaks in a TOF spectrum for the sake of this work. The result of the analysis using these two new methods fully confirms previously published results [32]. This is an important result, especially in the light of criticisms present in the NCS literature as far as data treatment from NCS experiments showing the anomaly of the scattering intensity is concerned [22–25, 47]. Moreover and most importantly, the presented results show that no broadening or lineshift is present of proton momentum distribution in $(NH_4)_2PdCl_6$ and $(NH_4)_2TeCl_6$, while the anomaly of the scattering intensity of protons is present in both systems. This result has interesting implications for further theoretical work in the field of anomalous scattering intensities as observed in neutron Compton scattering.

2. NCS scattering intensities in impulse approximation

2.1. Conventional data treatment scheme

In what follows only a brief description will be given. For a recent, rigorous theoretical treatment of neutron Compton scattering refer to the work by Mayers [20] or the recent review by Andreani *et al* [3]. In NCS the energy and momentum transfers from the neutron to the scattering nuclei are so high that the scattering process can be treated within the impulse approximation (IA) limit [21, 1, 40–43]. In the IA limit, i.e. in the limit of infinite momentum transfer q, the scattering function $S(q,\omega)$ reduces to a single peak centered at the recoil energy $\omega_r = q^2/2M$ of the corresponding nucleus of mass M, i.e. $S(q,\omega) = M/qJ(y)$, where y is the momentum p of the nucleus in the initial state projected onto the scattering vector q [21, 44]:

$$y = \mathbf{p}\cdot\hat{\mathbf{q}} = (M/q)\,(\omega - \omega_r) = (M/q)(\omega - q^2/2M) \quad (1)$$

where $\hat{\mathbf{q}}$ is the unit vector in the direction of the momentum transfer. $J(y)$ is the so-called Compton profile [1, 21] representing the momentum distribution of the scattering nucleus along y. For an isotropic system, in which $n(\mathbf{p})$ depends only on the magnitude of $\mathbf{p}$, $p = |\mathbf{p}|$, $J(y)$ in the IA limit is most commonly written as a normalized Gaussian form [20, 43, 3, 45, 40]:

$$J_{IA}(y) = \frac{1}{\sqrt{2\pi\sigma_p^2}}\exp\left(\frac{-y^2}{2\sigma_p^2}\right) \quad (2)$$

with standard deviation σ_p.

The corrections to the IA for the finite q of measurement, known as 'final state effects' (FSE), have been extensively discussed in recent reviews by Mayers [20] and Andreani [3]. From different approaches on how to account for FSE in NCS the method of Sears [21] is routinely incorporated in standard NCS data treatment [20]. Sears showed that the effects of finite momentum transfer q and energy transfer ω can be accounted for by expressing the neutron Compton profile $J(y)$ as

$$J(y) = J_{IA}(y) - \frac{M\langle\nabla^2 V\rangle}{36\hbar^2 q}\frac{d^3}{dy^3}J_{IA}(y) + \cdots \quad (3)$$

where $J_{IA}(y)$ is the IA result. $\langle\nabla^2 V\rangle$ is the mean value of the Laplacian of the potential energy of the atom [20].

For a real experimental situation the total number of neutrons detected for a given mass M in a time channel t is proportional to $J_M(y_M)$ convoluted with the mass-dependent instrumental resolution function in the y_M space, i.e. $R_M(y_M)$. Thus, for different masses present in the sample the total count rate $C(t)$ is ([20], equation (2.22))

$$C(\theta = \text{const}, t) = A'\frac{E_0(t)I[E_0(t)]}{q(t)} \times \sum_M I_M M J_M(y_M(t)) \otimes R_M(y_M(t)) \quad (4)$$

where A' is a mass-independent experimental constant and the factor $\frac{E_0(t)I[E_0(t)]}{q(t)}$ depends on the spectrum $I[E_0(t)]$ of initial neutron energies $E_0(t)$ and the momentum transfer $q(t)$, both mass-independent functions of time-of-flight t [20]. In equation (4) the nuclear momentum distribution of the mass M, $J_M(y_M(t))$, is given by the formula (3).

Integrated peak intensities I_M for a mass M of the scatterer are proportional to the bound scattering cross-sectional density $I_M = AN_M\sigma_M$, where $\sigma_M = 4\pi b_M^2$ is the total bound scattering cross section [46]. Hence, the measured value of $[I_H/I_X]_{exp}$ can be compared to the value of $[I_H/I_X]_{theor} = (N_H\sigma_H)/(N_X\sigma_X)$ calculated taking the tabulated [46] value of σ_M and the N_M, for a mass M, known from chemical formula and/or sample preparation. The ratio $R = \frac{[I_H/I_X]_{exp}}{[I_H/I_X]_{theor}}$ is smaller than unity in our experiments on hydrogen-containing materials (see, e.g., [11–16]), thus indicating the anomalous neutron Compton scattering from protons.

3. Nuclear momentum distribution from molecular motion

For a system of freely rotating molecules, neglecting the rotation–vibration interactions and any interplay of translational and internal coordinates, it is generally possible to separate the Hamiltonian, H, into three terms [51]:

$$H = H_{trans} + H_{rot} + H_{vibr} \quad (5)$$

where H_{trans} is related to the center-of-mass translations, H_{rot} to the molecular rotations and H_{vibr} to the internal vibrations of the nuclei. Colognesi *et al* [51] have developed a description of the single-particle momentum distribution for any nucleus belonging to an arbitrary freely rotating molecule. It was accomplished under the following three assumptions: (1) molecular rotations can be dealt with classically, (2) vibration displacements of nuclei from their equilibrium positions are small if compared with their average distances from the center of mass and (3) internal vibrations can be considered as purely harmonic. The description deals with the common situation encountered at room temperature,

in which the translational and rotational behavior of the free molecule can be described classically while, on the other hand, molecular vibrations are still quantized.

The translational contribution to the kinetic energy of a mass M in a molecule is simply equal to

$$\langle E_{\mathrm{k}}^{\mathrm{tra}}\rangle = \frac{1}{2}\frac{M}{M_{\mathrm{T}}}M_{\mathrm{T}}\vec{v}_{\mathrm{CM}}^{2} \tag{6}$$

where $\vec{v}_{\mathrm{CM}}$ is the molecule center-of-mass velocity [52, 51]. Making use of the classical equipartition theorem, we obtain $\langle E_{\mathrm{k}}^{\mathrm{tra}}\rangle = \frac{3}{2}\frac{M}{M_{\mathrm{T}}}k_{\mathrm{B}}T$.

The rotational contribution to the kinetic energy $\langle E_{\mathrm{k}}^{\mathrm{rot}}\rangle$ of a mass M in a molecule can be expressed, in the coordinate system coinciding with the molecular principal inertia axes, in the following way:

$$\langle E_{\mathrm{k}}^{\mathrm{rot}}\rangle = \tfrac{1}{2}Mk_{\mathrm{B}}T\sum_{i,j=1}^{3}(\hat{r}_i)R_{i,j}\hat{r}_j \tag{7}$$

where $\hat{r}$ is the unit vector in space and the tensor $R_{ni,j}$ is closely linked with the Sachs–Teller mass tensor [51, 52] for M, which often appears in the classical treatment of molecular rotations:

$$M_{i,j}^{-1} = R_{i,j} + M_{\mathrm{T}}^{-1}\delta_{i,j} \tag{8}$$

where M_{T} is the total mass of a molecule.

The vibrational contribution to the kinetic energy, $\langle E_{\mathrm{k}}^{\mathrm{vib}}\rangle$, can be worked out in the hypothesis that the displacements, $\vec{u}_M$, of the protons from their equilibrium positions, $\vec{d}_M$, are small in comparison with their average distances from the center of mass [51, 52]. Decomposing such displacements in normal modes q_λ by means of the amplitude vectors $\vec{C}_M^{\lambda}$ one obtains

$$\vec{u}_M = \sum_{\lambda=1}^{N_\lambda}\vec{C}_M^{\lambda}q_\lambda. \tag{9}$$

Then, $\sigma_M(\hat{r})^2$ for $\hat{r}$ parallel to the direction of the nuclear momentum $\vec{p}$ can be calculated using the following relation [51, 52]:

$$\hbar^2\sigma_M(\hat{r})^2 = M^2\sum_{\lambda=1}^{N_\lambda}(\vec{C}_M^{\lambda}\cdot\hat{r})^2\frac{\hbar\omega_\lambda}{2}\coth\left(\frac{\hbar\omega_\lambda}{2k_{\mathrm{B}}T}\right). \tag{10}$$

In general, the vibrational contribution is Gaussian but anisotropic and can be convoluted with translational and rotational to yield a total distribution function for an atom n, $J_n(y,\hat{r})$ characterized by an overall angular averaged variance $\sigma_n^2(\hat{r})$. Since the average value does not depend on the choice of the frame of reference, $\sigma_n^2(\hat{r})$ can be chosen so as to coincide with the molecular principal inertia axes, which is expressed by the following equation [51, 52]:

$$\hbar^2\sigma_n^2(\hat{r}) = M_n^2k_{\mathrm{B}}T/M_{\mathrm{T}} + M_n^2k_{\mathrm{B}}T\sum_{i,j=1}^{3}(\hat{r}_i)R_{ni,j}\hat{r}_j + M_N^2\sum_{\lambda=1}^{N_\lambda}(\vec{C}_n^{\lambda}\cdot\hat{r})^2\frac{\hbar\omega_\lambda}{2}\coth\left(\frac{\hbar\omega_\lambda}{2k_{\mathrm{B}}T}\right). \tag{11}$$

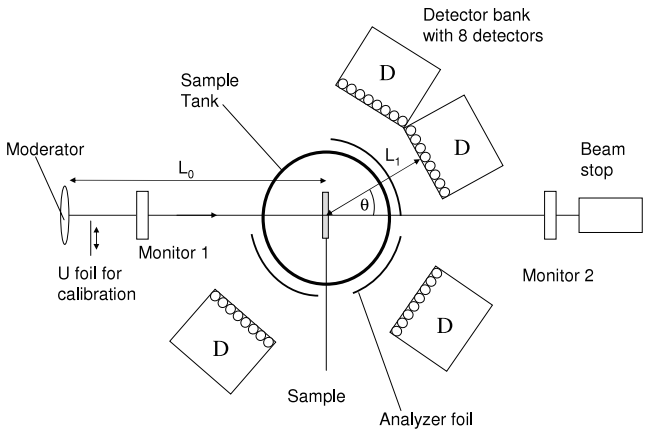

Figure 1. A schematic representation of the VESUVIO spectrometer at ISIS.

In NCS experiments performed on non-oriented samples only the angular average of $J_n(y,\hat{r})$ is observed [51]:

$$J_n(y) = \frac{1}{4\pi}\int \mathrm{d}\hat{r}\; J_n(y,\hat{r}). \tag{12}$$

The angular average in equation (12) must be performed numerically but the variance $\overline{\sigma_n^2}$ of $J_n(y)$ can be calculated analytically [51]:

$$\overline{\sigma_n^2} = \tfrac{1}{3}(\sigma_n(\hat{x})^2 + \sigma_n(\hat{y})^2 + \sigma_n(\hat{z})^2). \tag{13}$$

where σ_n^2 is defined in equation (11).

4. Materials and methods

4.1. The VESUVIO spectrometer at ISIS spallation source

The VESUVIO spectrometer at the ISIS neutron spallation source is an inverted geometry time-of-flight instrument [20]. The sample is exposed to a polychromatic neutron beam characterized by an incident neutron energy spectrum $I(E_0)$. Incident neutrons having initial energy E_0 travel a distance L_0 from the pulsed source to the sample. After scattering at an angle θ, neutrons of final energy E_1 travel a distance L_1 to the detector position (figure 1). The TOF spectrum is obtained by taking the difference of two spectra: one with a thin foil of a neutron absorbing material between the sample and the detector and one without the foil. In most NCS experiments a thin gold foil, absorbing neutrons with final energy $E_1 = 4.9$ eV, is used [20]. The NCS data presented here were recorded with the so-called old detector set-up, i.e. the forward scattering detectors are Li glass detectors, grouped in four banks of eight detectors each.

4.2. Experimental details

Ammonium hexachloropalladate (IV) was purchased from the Alfa Aesar Company (article no. 11042, 99.9% (metal basis)). Ammonium hexachlotellurate (IV) was the product of Sigma Aldrich (article no. 572756-5G, 99.9% (metal basis)). Both samples were purchased as friable powders. The samples

were weighed before and after each NCS measurement. After the completion of the NCS experiment the analysis of structure and composition of both samples was conducted. The x-ray powder diffraction (XRD) analyses were performed, showing only small amounts (<5%) of side phases [32]. Additionally, the combustion method was applied for the determination of the hydrogen content. The hydrogen content was 2.3 wt% and 2.1 wt% for $(NH_4)_2PdCl_6$ and $(NH_4)_2TeCl_6$, respectively, in good agreement with the theoretical values calculated from the chemical formula [32]. Both samples were contained in sachets made of very thin aluminum foil, giving negligible scattering intensities from aluminum [32]. All measurements were performed at the temperature of 295 K. The integrated proton current during the runs was 3577 and 7183 μA h for $(NH_4)_2PdCl_6$ and $(NH_4)_2TeCl_6$, respectively [32]. Only forward scattering time-of-flight (TOF) spectra for both samples were recorded for 32 detectors at scattering angles θ in the range from 34° to 67° [32]. TOF spectra for both samples exhibit two recoil peaks: a broad and relatively strong peak at smaller scattering times due to scattering from protons, and a tall and narrow peak at higher scattering times due to chlorine (Cl), nitrogen (N) and metal (Me = Pd, Te) [32].

5. *Ab initio* calculation of proton momentum distribution

There is strong experimental evidence from previous NCS experiments [32] that molecular dynamics of the ammonium ion is very well decoupled from the dynamics of the rest of the lattice in $(NH_4)_2PdCl_6$ and $(NH_4)_2TeCl_6$. This evidence is provided by the fact that in both systems the proton momentum distribution, as measured in the NCS experiment, is equal to 5.0 Å^{-1} and thus independent of the electronic structure and nuclear dynamics of the crystalline sublattice containing $TeCl_6^{2-}$ and $PdCl_6^{2-}$ octahedra [32]. Thus, in the *ab initio* calculation of proton momentum distribution in $(NH_4)_2PdCl_6$ and $(NH_4)_2TeCl_6$ presented below the NH_4^+ molecule in hexachlorometallates was treated as an isolated freely rotating ion. Standard deviations of momentum distribution $\sigma(M)$ were calculated from the mean kinetic energy of an atom $\langle E_M^{\mathrm{k}}\rangle$, taking into account vibrational, rotational and translational contributions (see equation (11)). The total number of vibrational modes N_λ is equal to $3N - 6$. With $N = 5$ we get nine normal modes. However, due to tetrahedral symmetry reasons we observe only four vibrational frequencies [55]: 1, symmetric N–H stretching mode ($\omega_1 = 3040$ cm^{-1}); 2, symmetric HNH deformation mode ($\omega_{2,3} = 1680$ cm^{-1}); 3, antisymmetric N–H stretching mode ($\omega_{4,5,6} = 3145$ cm^{-1}); 4, antisymmetric HNH deformation mode ($\omega_{7,8,9} = 1400$ cm^{-1}). For the vibrational contribution for each mode λ eigenfrequencies ω_λ and the eigenvectors q_λ were calculated in Gaussian 98 using the DFT method with B3LYP triple-ζ basis set 6-311 + G(d, p) [56] with diffuse and polarization functions added.

The following remark is in order as far as the choice of the method and basis set for the vibrational calculation is concerned. Vibrational frequencies calculated in Gaussian 98 using the DFT method are known to exhibit systematic errors and scaling factors are introduced to account for this [53]. Usually, three different scaling factors are calculated based on the comparison of theoretically calculated vibrational frequencies with experimental values: vibrational frequency scaling factor, the scaling factor for low-frequency vibrations and zero-point vibrational energy scaling factor [54]. The scale factor c to use with vibrational frequencies is calculated by making a least-squares fit of the scaled harmonic frequencies to the experimental fundamentals, i.e. minimizing the following sum [54]:

$$\Delta = \sum_{i=1}^{N} (c\omega_i^{\mathrm{theor}} - \omega_i^{\mathrm{exp}})^2 \tag{14}$$

where N is the number of frequencies included in the optimization. The root-mean-square (RMS) error is [54]

$$\mathrm{RMS} = \sqrt{\frac{\Delta}{N}}. \tag{15}$$

A program in MATLAB has been written that calculates the scaling factor c for the specific case of the NH_4^+ molecular ion from equation (14) together with RMS from equation (15), given the experimental values of vibrational frequencies [55]. Of all hybrid DFT methods, the B3LYP functional is the most widely used [57]. It is most often combined with the basis set 6-31G(d) and it has been used for almost a decade with consistently good results. Since the mid-1990s, however, another basis set, namely the triple-ζ basis set 6-311 + G(d, p), has been used which has recently been shown to outperform other datasets in the calculation of vibrational frequencies [54]. Thus, the basis set 6-311 + G(d, p) was chosen for the calculation of the vibrational frequencies of NH_4^+. The scaling factor c calculated for NH_4^+ using experimental values of vibrational frequencies [55] was 0.9149 with RMS error equal to 57.13. This value is somewhat different from the value of the scaling factor for the basis set 6-311 + G(d, p) calculated by Andersson *et al* [54], being 0.9613 with RMS error equal to 33. However, the calculation of Andersson *et al* [54] was performed for a set of molecules not comprising the NH_4^+. Moreover, we have performed similar calculations for basis sets 6-31G(d) and all sets from 6-311G up to 6-311G++ (3df, 3pd), always with almost identical results for the scaling factor c. Also, the RMS error of our calculation (57.13) turns out to be in the middle of the range of RMS errors calculated by Andersson *et al* [54] (ranging from 32 to 95) for all triple-ζ 6-311G basis sets. This, in combination with the other facts mentioned above, justifies the use of the numerical value of c equal to 0.9149 for the calculation of vibrational frequencies. The values of the scaled calculated NH_4^+ vibrational frequencies are compared to the experimental values [55] and listed in table 1.

From the Gaussian 98 output the nuclear displacements in the NH_4^+ molecule were calculated using the freely available program ACLIMAX 5.5.0 [58, 53] taking into account the scaling factor $c = 0.9149$. The nuclear displacements that ACLIMAX uses to generate the INS spectra are the normalized mass-weighted Cartesian displacement coordinates as defined by Wilson *et al* [59]. Gaussian 98 writes a non-standard output,

Table 1. The values of the scaled (using the scaling factor $c = 0.9149$) calculated NH_4^+ vibrational frequencies compared to the experimental values [55].

Mode no.	$\omega_{\text{theor}}c$ (cm^{-1})	ω_{exp} (cm^{-1})
1	3085	3040
2	1580	1680
3	3179	3145
4	1363	1400

Table 2. Standard deviations of proton momentum distribution calculated neglecting rotational and translational contributions for NH_4^+ from Gaussian 98 output using ACLIMAX and a program written in MATLAB using equation (10). The average isotropic momentum calculated from vibration using equation (13) is given in the last column.

Atom	$\sigma_M(\hat{x})$ (Å^{-1})	$\sigma_M(\hat{y})$ (Å^{-1})	$\sigma_M(\hat{z})$ (Å^{-1})	$\overline{\sigma_M}$ (Å^{-1})
N	14.003	9.644	9.6066	9.6938
H1	1.0078	4.8038	4.8016	4.8075
H2	1.0078	4.824	4.8307	4.8245
H3	1.0078	4.813	4.8222	4.7995
H4	1.0078	4.7731	4.7887	4.7806

Table 3. Total, translational, rotational and vibrational mean kinetic energies of a single nucleus in freely rotating ammonium ion at room temperature.

Atom	$E_{\text{kin}}^{\text{tot}}$ (meV)	$E_{\text{kin}}^{\text{trans}}$ (meV)	$E_{\text{kin}}^{\text{libr}}$ (meV)	$E_{\text{kin}}^{\text{vib}}$ (meV)
N	71.8046	30.1216	0	41.6829
H1	155.4629	2.1679	9.6899	143.6051
H2	156.7906	2.1679	9.6899	144.9328
H3	155.8982	2.1679	9.6899	144.0404
H4	154.0627	2.1679	9.6899	142.2050

Table 4. Standard deviations of proton momentum distribution calculated including vibrational, rotational and translational contributions for NH_4^+ using equation (10). The average isotropic momentum calculated from vibration using equation (13) is given in the last column.

Atom	$\sigma_M(\hat{x})$ (Å^{-1})	$\sigma_M(\hat{y})$ (Å^{-1})	$\sigma_M(\hat{z})$ (Å^{-1})	$\overline{\sigma_M}$ (Å^{-1})
N	12.66	12.6315	12.698	12.6632
H1	4.9982	4.9961	5.0018	4.9987
H2	5.0177	5.0241	5.0182	5.02
H3	5.0071	5.0159	4.9941	5.00569
H4	4.9687	4.9838	4.9759	4.97614

see [60]. ACLIMAX takes this into account and renormalizes the displacement vectors [58, 53]. The output ACLIMAX displacement vectors $\vec{x}_n^{\lambda}$ are normalized such that the sum of squares of all vectors is equal to unity, which reflects the fact that the molecular center of mass does not move during the molecular vibration [53]. In order to transform the unitless normalized displacement vectors $\vec{x}_n^{\lambda}$ into displacements $\vec{w}_n^{\lambda}$ in units of square ångströms, the following transformation must be performed (see equation (4.31) in [53]):

$$\vec{w}_n^{\lambda} = \sqrt{\frac{16.9}{M\omega_{\lambda}}}\vec{x}_n^{\lambda} \tag{16}$$

where M is the nuclear mass in amu and ω_{λ} is the frequency of a mode λ in cm^{-1}. From them it is possible to work out the amplitude vectors [51, 52], C_n^{λ}, defined in equation (9), which have the physical dimensions of [mass]$^{-1/2}$:

$$\vec{C}_n^{\lambda} = \frac{\vec{w}_n^{\lambda}}{[\sum_{n=1}^{N} M_n|\vec{w}_n^{\lambda}|^2]^{1/2}}. \tag{17}$$

From $\vec{C}_n^{\lambda}$ the values of $\sigma_n(\hat{r})$ were calculated for each nucleus in NH_4^+. The calculation of $\vec{w}_n^{\lambda}$, $\vec{C}_n^{\lambda}$ and $\sigma_n(\hat{r})$ was performed using a program written in MATLAB that takes as an input ACLIMAX output files. Standard deviations of nuclear momentum distribution were first calculated neglecting rotational and translational contributions using equation (10). The average isotropic momentum was calculated from molecular vibration using equation (13). The results are shown in table 2. The next stage of the calculation was the inclusion of translational and rotational energies into the total nuclear kinetic energy. The kinetic energies of translational, rotational and vibrational motion were calculated per nucleus using equation (11). Their values are given in table 3. The standard deviations of nuclear momentum distribution along x, y, z calculated including translational, librational and vibrational kinetic energies were next calculated per nucleus using equation (11). Their values are given in table 4.

Both hexachlorometallates were measured as powders. Thus, the NCS observable in both cases is simply the angular average of the three-dimensional nuclear momentum distribution. As discussed above (see section 3), the variance of such an observable momentum distribution can be calculated analytically by equation (13). The analytically calculated averaged standard deviation of nuclear momentum distribution in NH_4^+ is given in the last column of table 4 for the N nucleus and each of four protons in the molecule. Now, even though the observable standard deviation of momentum distribution can be calculated analytically, the exact lineshape of the momentum distribution function $J(y)$ must still be calculated numerically (see section 3). Thus, for instance, even if a three-dimensional momentum distribution is very well described as a multivariate Gaussian, the angular averaged momentum distribution will not be a Gaussian. There is, however, one important exception to this rule: the case of a multivariate Gaussian with standard deviations $\sigma_M(\hat{x})$, $\sigma_M(\hat{y})$ and $\sigma_M(\hat{z})$ being equal. From table 4 it is evident that it is exactly the case for the *ab initio* calculation presented here. Thus, for NH_4^+ at 300 K the nuclear momentum distribution can be, to a very good approximation, treated as a Gaussian function [3, 51, 52, 20] $J_H(y)$ with $\overline{\sigma_H} = 5.0$ Å^{-1}.

The ammonium ion's rotational and translational energies at room temperature are also not much different from those calculated by Colognesi *et al* for free rotating ammonia molecules using a detailed model [51]. The calculation shows that the vibrational, rotational and translational energies of protons at room temperature in NH_3 are 138.82, 12.45 and 2.30 meV, respectively [51]. Our values calculated for protons in the ammonium ion are 143.7, 9.6899 and 2.1679 meV on average.

The average value of standard deviation of momentum distribution calculated in the *ab initio* method for a nitrogen nucleus in NH_4 is 12.66 Å^{-1}. The values of vibrational,

rotational and translational energies at room temperature are 41.6829, 0 and 30.1216 meV, respectively. The similar figure for NH_3 yields 31.46, 1.43 and 31.89 meV at room temperature [51]. The obvious small difference in these energies comes from the fact that, whereas NH_4 is a spherical top with center of mass centered at the position of nitrogen, the NH_3 is a rotating symmetric top molecule.

6. Nuclear momentum distribution from the NCS measurement

In order to compare the results of the *ab initio* momentum distribution calculation presented above with the experimental results obtained for $(NH_4)_2PdCl_6$ and $(NH_4)_2TeCl_6$, first the hypothesis about the Gaussian form of the proton momentum distribution was tested. A new NCS data reduction scheme has been applied [5] that uses the Gram–Charlier series [3, 4]. The entire TOF spectrum, containing multiple recoil peaks from different masses M is fitted directly in TOF with the function $C(t)$ being a combination of the Gram–Charlier expansion for protons, J_H, and the sum of Gaussian momentum distribution functions for $M \neq M_H$, J_M, both convoluted with mass-dependent resolution functions, R_M. Additionally, FSE contributions to both Gaussian and non-Gaussian J_M are accounted for by including terms proportional to $1/qH_3$. The resulting expression to fit the entire TOF spectrum is of the following form:

$$C(\theta = \text{const}, t) = A' \frac{E_0 I[E_0]}{q} \times \left[J_H(x_H) \otimes R_H(x_H) + \sum_{M \neq M_H} J_M(x_M) \otimes R_M(x_M) \right], \tag{18}$$

where

$$J_H(x_H) = \frac{\exp(-x_H^2)}{\sqrt{2\pi\sigma_H^2}} \left(1 + \frac{c_4}{32} H_4(x_H) - \frac{k}{q} H_3(x_H) \right) \tag{19}$$

and

$$J_M(x_M) = \frac{\exp(-x_M^2)}{\sqrt{2\pi\sigma_M^2}} \left(1 - \frac{k}{q} H_3(x_M) \right) \tag{20}$$

with $x_M = (y_M - y0_M)/(\sigma_M\sqrt{2})$, where $y0_M$ is the shift of the position of the maximum of a nuclear momentum distribution from the center of the recoil line and σ_M is the standard deviation of the momentum distribution for a mass M. FSE expansion in the limit of a harmonic potential leads to a very useful expression of the FSE coefficient k in the expansion given by equation (18), $k = \sigma\sqrt{2}/12$. Thus, fitting of the recoil peaks in a harmonic approximation does not require any extra fitting parameter to describe FSE.

The following protocol was applied to reduce the entire NCS TOF spectra. The widths of nuclear momentum distributions of nuclei other than protons were fixed in fitting. The width for nitrogen was set equal to the values of 12.663 $Å^{-1}$, calculated from semiclassical molecular translation, rotation and vibration analyses. The standard deviations of momentum distributions σ_p(Me) for Me = Pd, Te and σ_p(Cl) for Cl were, as in previous work [32], calculated from the Debye solid model using Debye temperatures reported by Gupta *et al* being 120 K and 105 K for $(NH_4)_2PdCl_6$ and $(NH_4)_2TeCl_6$, respectively [33]. Based on these values of Debye temperatures the calculated values of standard deviations of momentum distributions of Pd, Te and Cl were $\sigma_p(\text{Pd}) = 25.9$ $Å^{-1}$, $\sigma_p(\text{Te}) = 28$ $Å^{-1}$ and $\sigma_p(\text{Cl}) = 16.4$ and 15.2 $Å^{-1}$ for $(NH_4)_2PdCl_6$ and $(NH_4)_2TeCl_6$, respectively. It is worth mentioning that these values agree very well with the values obtained from semiclassical molecular translation, rotation and vibration analyses for isolated $PdCl_6^{2-}$ and $TeCl_6^{2-}$ octahedra. The Gaussian 98 calculation at the HF level of the theory using the 3-21G basis set gave $\sigma_p(\text{Pd}) = 26.9$ $Å^{-1}$, $\sigma_p(\text{Te}) = 29.2$ $Å^{-1}$, and $\sigma_p(\text{Cl}) = 15.4$ $Å^{-1}$ and $\sigma_p(\text{Cl}) = 15.0$ $Å^{-1}$ for $(NH_4)_2PdCl_6$ and $(NH_4)_2TeCl_6$, respectively. These values changed by only less than 5% by adding the nearest neighbors in the cubic lattice.

Table 5. The weighted (over the whole set of forward scattering detectors on VESUVIO) average values of: widths of momentum distributions σ_H, the shifts of the momentum distribution peak of protons $y0_H$ and the Gram–Charlier expansion coefficients $c4_H$ obtained of the proton momentum distribution in ammonium hexachloropalladate and ammonium hexachlorotellurate.

Sample	σ_H ($Å^{-1}$)	$y0_H$ ($Å^{-1}$)	$c4_H$
$(NH_4)_2PdCl_6$	5.0 ± 0.02	0.00 ± 0.04	0.03 ± 0.01
$(NH_4)_2TeCl_6$	4.98 ± 0.02	0.00 ± 0.04	0.02 ± 0.01

As in the previous study [32], during the fitting of scattering intensities an additional linear constraint was imposed on fitting parameters: the ratio of scattering intensities from Cl, N and Pd or Te, respectively, was fixed using the tabulated scattering cross-sectional values and the sample stoichiometry. This ratios are

$$I_{\text{Cl}}{:}I_{\text{N}}{:}I_{\text{Te}} = 6 \times 16.8{:}2 \times 11.5{:}1 \times 4.32, \quad I_{\text{Cl}}{:}I_{\text{N}}{:}I_{\text{Pd}} = 6 \times 16.8{:}2 \times 11.5{:}1 \times 4.5 \tag{21}$$

for $(NH_4)_2PdCl_6$ and $(NH_4)_2TeCl_6$, respectively.

Additionally, for all nuclei with masses M other than protons the shifts $y0_M$ of the Compton profiles from the centers of the recoil lines for masses M were fixed to $y0_M = 0$ in fitting. Thus, the parameters free in fitting were scattering intensities I_H and I_M for protons and other nuclei, respectively, the proton recoil peak shift $y0_H$, standard deviation of proton momentum distribution σ_H and the values of the fourth Hermite polynomials coefficient, $c4_H$. It turns out that in Gram–Charlier expansion $c_4 = \delta/3$, where δ is the kurtosis of the single-particle momentum distribution, $\delta = (\mu_4 - 3\langle\sigma^2\rangle^2)/\langle\sigma^2\rangle^2$, with μ_4 being the fourth moment of the momentum distribution [4, 6]. A sequential fit was first performed and the values of σ_H and $c4_H$ fitted detector by detector. Then, a weighted average (over the whole set of forward scattering detectors) was calculated of σ_H and $c4_H$. The results of this calculation are shown in table 5.

In figure 2 are shown the values of σ_H obtained from fits to NCS data recorded for ammonium hexachloropalladate

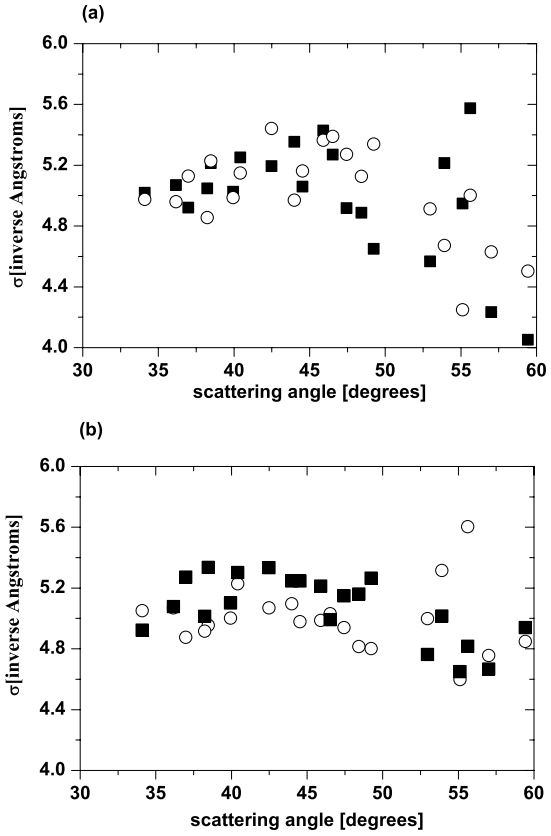

Figure 2. Comparison of σ_H values obtained in two data treatment schemes: purely Gaussian momentum distribution fits to NCS data (full squares) and fits using Gram–Charlier expansions (open circles). (a) Results from $(NH_4)_2PdCl_6$, (b) results from $(NH_4)_2TeCl_6$.

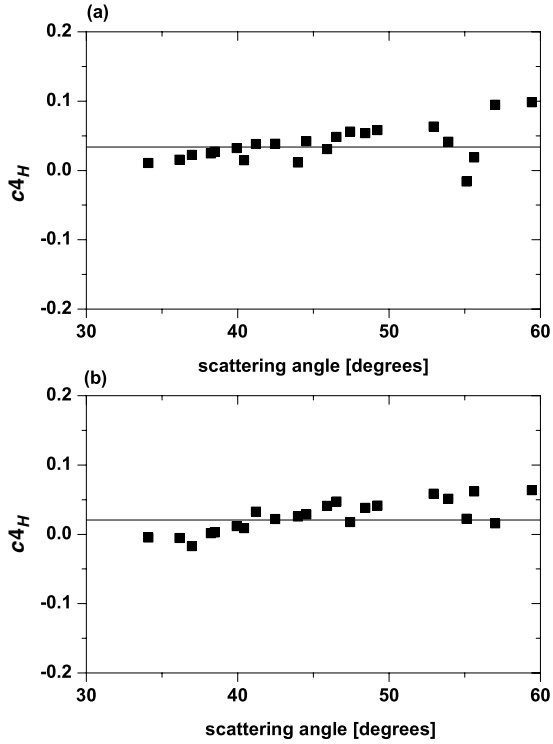

Figure 3. Comparison of values of kurtosis of proton momentum distribution $c4_H$ obtained using Gram–Charlier expansions. (a) Results from $(NH_4)_2PdCl_6$, (b) results from $(NH_4)_2TeCl_6$.

and ammonium hexachlorotellurate using: (i) purely Gaussian Compton profiles and (ii) Gram–Charlier expansions. The values fitted by the expansion are almost identical to the Gaussian approximation for both systems (see table 5) and agree very well with the value of σ_H obtained from the *ab initio* calculation described above.

The proton momentum distribution analysis based on Gram–Charlier expansion reveals an interesting effect concerning the anharmonicity of the momentum distributions. The values of the kurtosis of the momentum distributions are not vanishing in both ammonium hexachloropalladate and ammonium hexachlorotellurate showing slightly non-Gaussian momentum distribution, as shown in figure 3. The weighted average of the kurtosis of the momentum distribution, $c4_H$, is equal to 0.03 ± 0.01 and 0.02 ± 0.01 for $(NH_4)_2PdCl_6$ and $(NH_4)_2TeCl_6$, respectively, thus equal within the statistical accuracy of the calculation. As shown in figure 3 the kurtosis values, as plotted against the scattering angles, seem not to show any pronounced trend.

Comparison of fits of the longitudinal, $J(y)$, and radial, $4\pi p^2 n(p)$, momentum distributions to the $(NH_4)_2PdCl_6$ and $(NH_4)_2TeCl_6$ data was shown in figures 4 and 5, respectively. Both radial and longitudinal momentum distributions for both ammonium salts have been plotted using average values obtained from sequential fits of Gram–Charlier expansions performed detector by detector and given in table 5. Additionally, Gaussian $J(y)$, and $4\pi p^2 n(p)$ momentum distributions for $\sigma_H = 5$ Å^{-1} have been plotted in these figures as dashed lines. In both longitudinal momentum distribution functions $J(y)$ final-state effects (FSE) are included through Sears expansion. The magnitude k of the FSE is fixed at $k = \frac{\sqrt{2}\sigma_H}{12}$. The FSE is plotted for the magnitude of the momentum transfer $q = 45$ Å^{-1}. In the radial momentum distributions the FSE is omitted.

To sum up, no systematic increase of the widths and kurtosis of momentum distributions with increasing scattering angle is observed in both $(NH_4)_2PdCl_6$ and $(NH_4)_2TeCl_6$. As the scattering angle increases the scattering time decreases according to the formula given by Sears [21, 1, 37–39]. The scattering time, calculated for standard deviation of proton momentum distribution $\sigma_H = 5$ Å^{-1}, is equal to approx. 1.1 fs at the scattering angle of 30° and to approx. 0.3 fs [32]. Thus, any increase of the value of standard deviation and/or kurtosis with increasing scattering angle would point to possible effects of the scattering process taking place at shorter times on the proton momentum distribution. Thus, the main result of the analysis of proton momentum distributions in both ammonium salts is that no extra broadening is present that would have been due to ultra-fast kinetics of the scattering process postulated in the literature [34–36].

7. Scattering intensities from the NCS measurement

As described in previous work on NCS data reduction, both the Dorner [26, 48–50] and center-of-peak [27] methods can

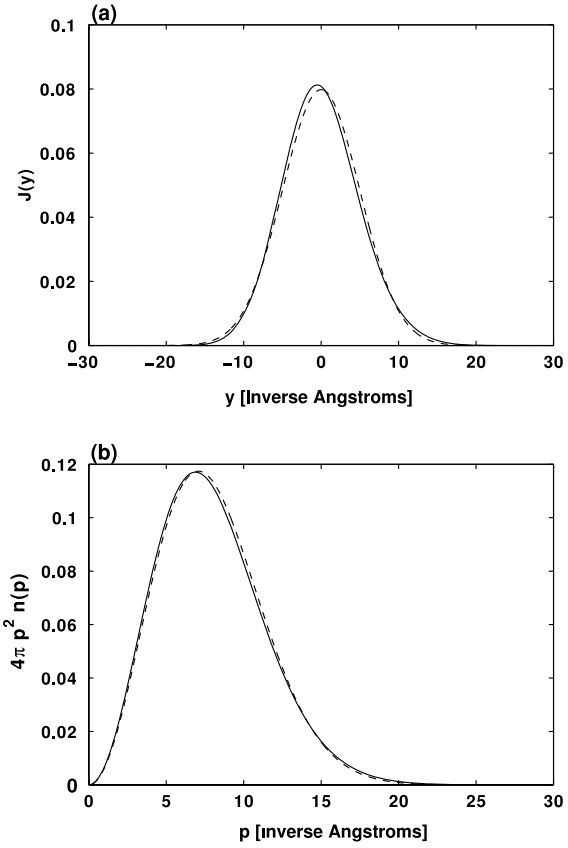

Figure 4. Comparison of fits to the $(NH_4)_2PdCl_6$ data of the longitudinal, $J(y)$, and radial, $4\pi p^2 n(p)$, momentum distributions. The functions $J(y)$ and $n(p)$ are plotted for the average values of standard deviation of momentum distributions σ_H and Gram–Charlier expansion coefficients $c4_H$ given in table 5. Additionally, Gaussian $J(y)$, and $4\pi p^2 n(p)$ momentum distributions for $\sigma_H = 5$ Å^{-1} have been plotted as dashed lines. In both longitudinal momentum distribution functions $J(y)$ final-state effects (FSE) are included through Sears expansion. The magnitude k of the FSE is fixed at $k = \frac{\sqrt{2}\sigma_H}{12}$. The FSE is plotted for the magnitude of the momentum transfer $q = 45$ Å^{-1}. In the radial momentum distributions the FSE is omitted.

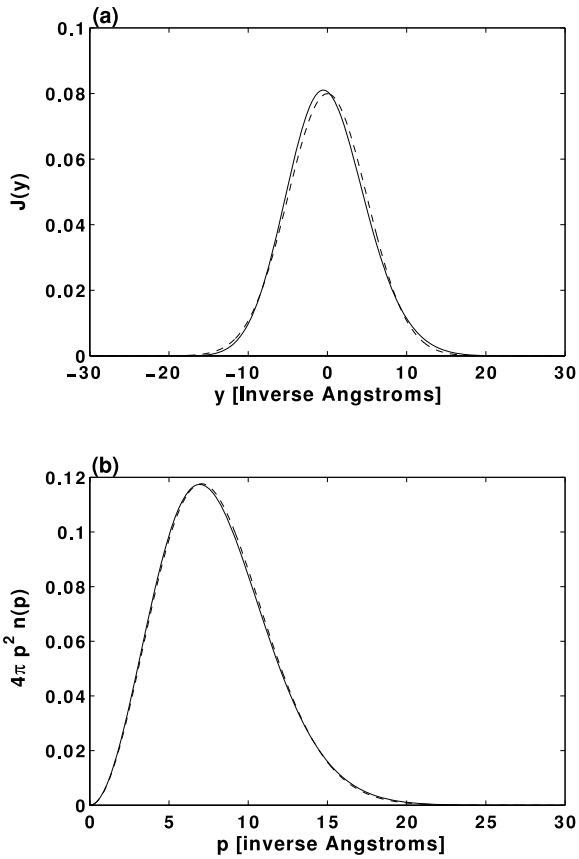

Figure 5. Comparison of fits to the $(NH_4)_2TeCl_6$ data of the longitudinal, $J(y)$, and radial, $4\pi p^2 n(p)$, momentum distributions. The functions $J(y)$ and $n(p)$ are plotted for the average values of standard deviation of momentum distributions σ_H and Gram–Charlier expansion coefficients $c4_H$ given in table 5. Additionally, Gaussian $J(y)$ and $4\pi p^2 n(p)$ momentum distributions for $\sigma_H = 5$ Å^{-1} have been plotted as dashed lines. In both longitudinal momentum distribution functions $J(y)$ final-state effects (FSE) are included through Sears expansion. The magnitude k of the FSE is fixed at $k = \frac{\sqrt{2}\sigma_H}{12}$. The FSE is plotted for the magnitude of the momentum transfer $q = 45$ Å^{-1}. In the radial momentum distributions the FSE is omitted.

be applied only under the assumption that a TOF spectrum contains well-separated recoil peaks. In the TOF spectra of $(NH_4)_2PdCl_6$ and $(NH_4)_2TeCl_6$ there are two relatively well-resolved peaks: the proton peak at lower values of time of flight, and a composite peak coming from neutron recoil off heavier masses [32] at higher values of time of flight. Under such experimental situations it is still possible to apply both the center-of-peak and Dorner methods to the NCS data. One can introduce a fictitious mass X being a weighted average of masses of the ratio of Cl, N and Pd or Te, with weights given by bound scattering cross sections multiplied by the number densities of masses in the samples:

$$M_X = \frac{6\times\sigma(\mathrm{Cl})\times M_{\mathrm{Cl}} + 2\times\sigma(\mathrm{N})\times M_{\mathrm{N}} + 1\times\sigma(\mathrm{Me})\times M_{\mathrm{Me}}}{6\times\sigma(\mathrm{Cl}) + 2\times\sigma(\mathrm{N}) + 1\times\sigma(\mathrm{Me})} \quad (22)$$

where M = Pd, Te. The value of M_X was equal to 34.03 and 34.72 amu for $(NH_4)_2PdCl_6$ and $(NH_4)_2TeCl_6$, respectively. Following this a standard CA fitting can be performed for two masses only: M_H and M_X. In the case of the center-of-peak method an *a priori* knowledge of the widths of the nuclear momentum distribution is required [27]. In the concrete case of $(NH_4)_2PdCl_6$ and $(NH_4)_2TeCl_6$ the width of the proton momentum distribution was fixed at a value of 5.0 Å^{-1} obtained from the *ab initio* analysis and a first CA fit was performed detector by detector with the width σ_X for M_X as a floating fitting parameter. Then, a weighted average of σ_X was calculated for the purpose. Finally, the scattering cross-sectional densities I_H and I_X were calculated for individual scattering angles θ for time-of-flight values corresponding to the center of recoil peaks for H and X.

The proposed extension of the Dorner method to the case of TOF spectra with multiple recoil peaks relies on the

following observation. As the Waller–Froman Jacobian used in the Dorner scheme differs from unity practically for H only [49, 50] the pointwise multiplication with the Jacobian is important for the proton scattering function only [50]. The Jacobian calculated for $M > 1$ amu is, up to numerical precision, equal to unity across the entire domain of energy transfer ω for the scattering function of nuclei with $M > 1$ amu. As a consequence, there is no need to separate recoil peaks for heavier masses in ω domain and the introduction of a fictitious mass M_X is fully justified to describe a composite recoil peak. However, unlike in the center-of-peak method, a clear peak separation between protons and the composite recoil peak is still required. Thus, the Dorner scheme was applied to reduce the NCS data from $(NH_4)_2PdCl_6$ and $(NH_4)_2TeCl_6$ only for scattering angles $\theta > 45°$. Two scattering functions were introduced in the energy transfer domain for protons and the fictitious mass, respectively. They were pointwise multiplied with the Waller–Froman Jacobians and finally numerically integrated in the ω domain to get the experimental scattering intensities for H and X, respectively [26, 48, 50].

The quantity of interest that was subject to experimental test was the reduction factor R of the neutron scattering intensities from protons I_H. R was defined as the ratio

$$R = \frac{\left[I_H/I_X\right]_{\text{exp}}}{\left[I_H/I_X\right]_{\text{theor}}} \tag{23}$$

where I_X was defined as the scattering intensity from the fictitious mass M_X. The quantity $[I_H/I_X]_{\text{exp}}$ was measured for different scattering angles θ and compared to the value of $[I_H/I_X]_{\text{theor}}$ calculated taking the tabulated scattering cross sections σ_M and the N_M for N, Cl and Pd or Te known from sample chemical formula. In both samples, R was found to be smaller than unity. Moreover, all three methods of NCS data reduction give qualitatively the same result: the anomaly decreases with decreasing θ and, at $\theta \sim 35°$, almost vanishes. The dependence of the magnitude of the anomaly on the scattering angle (scattering time) is shown in figure 6.

From figure 6 it is also evident that all three methods of NCS data reduction give very similar results over the entire range of forward scattering angles θ from 30° to 60°. The following tendency is visible. The values of the scattering intensity reduction factor R calculated from the conventional CA method tend to lie in the middle between the values obtained from the 'center-of-peak' method being systematically slightly bigger and the values obtained from the Dorner method being slightly lower. There may be small systematic differences between the CA data treatment on the one side and the 'center-of-peak' and Dorner methods on the other coming from the fact that the latter two methods use a fictitious mass M_X instead of fully resolving the recoil peaks from N, Cl and Me. This small systematic difference is a consequence of the simple fact that, although the N, Cl and Me peaks are not resolved, the mathematical form of the curve describing the shape of the combined heavy mass peak would be a sum of Voigt (being a convolution of a Gaussian momentum distribution function with the instrument resolution function, see, e.g., [20]) profiles of individual masses. This sum is not identically equal to a single Voigt function representing the recoil peak shape of the fictitious mass M_X. On the overall, however, the agreement between all three methods is very good, reinforcing the evidence of the experimental findings reported in a previous paper: an anomalous neutron Compton scattering effect from protons and thus confirming the previous result from $(NH_4)_2PdCl_6$ and $(NH_4)_2TeCl_6$ [32].

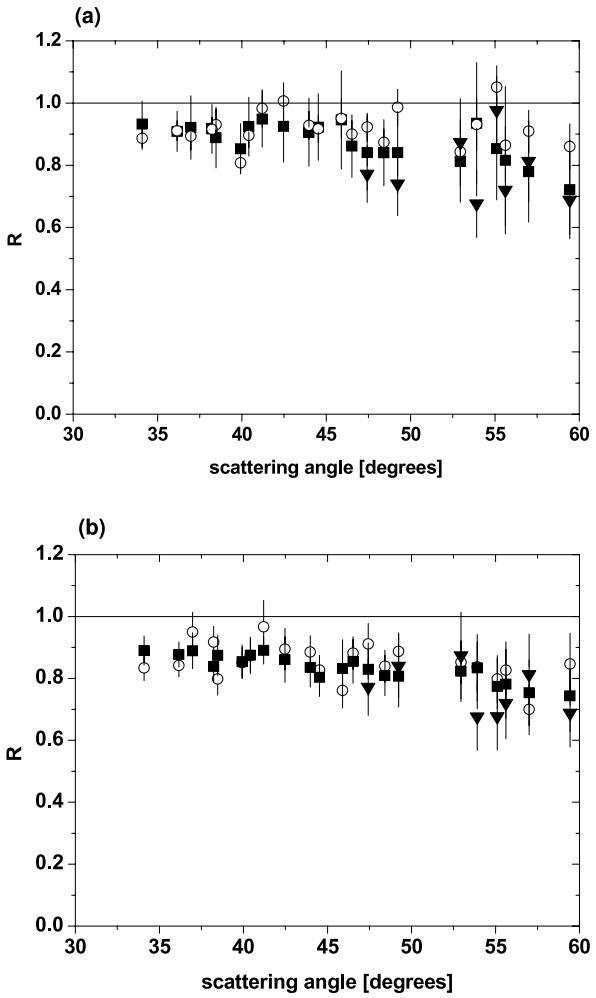

Figure 6. Reduction factor R of the proton scattering intensities as a function of scattering angle θ. Three different NCS data reduction schemes are compared: open circles—new 'center-of-peak' method, full squares—conventional CA method, full triangles—Dorner method. (a) Results from $(NH_4)_2PdCl_6$, (b) results from $(NH_4)_2TeCl_6$.

The anomalies of the scattering intensities of protons in $(NH_4)_2PdCl_6$ and $(NH_4)_2TeCl_6$ calculated using the Gram–Charlier expansion were compared with previous results where the recoil peaks of protons were treated as a purely Gaussian function. The plot of the anomalies calculated using both methods to account for the proton momentum distribution is shown in figure 7. In both $(NH_4)_2PdCl_6$ and $(NH_4)_2TeCl_6$, the anomalies are equal within the statistical accuracy of the measurements over the entire range of forward scattering angles (i.e. between 30° and 60°). Thus, inclusion of anharmonic contributions to proton momentum distribution

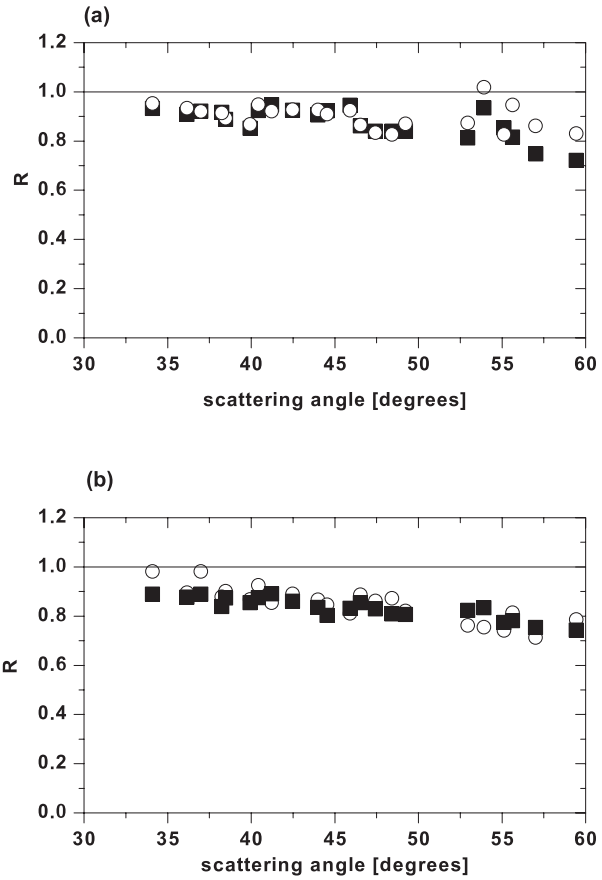

Figure 7. Reduction factor R of the proton scattering intensities. Scattering intensities of protons were obtained in the framework of the convolution approximation with proton Compton profile fitted either with a Gaussian function (full squares) or with the Gram–Charlier expansion (open circles). Results are shown for (a) $(NH_4)_2PdCl_6$ and (b) for $(NH_4)_2TeCl_6$.

does not seem to have any effect on the calculated magnitude of the anomaly of proton scattering intensities in both systems.

8. Discussion

The main result of the NCS work presented in this paper is the success of the *ab initio* method to explain the proton momentum distribution in $(NH_4)_2PdCl_6$ and $(NH_4)_2TeCl_6$. The second moment of proton momentum distribution in ammonium hexachloropalladate and ammonium hexachlorotellurate calculated from experimental data using both Gaussian and Gram–Charlier expansion taking into account non-harmonic contributions agrees very well with the value obtained from the *ab initio* calculation of the proton momentum distribution in an isolated NH_4^+ molecule. The *ab initio* calculation took into account molecular translation, rotation (classically) and vibration (quantum mechanically) of an isolated molecule in a ground state without taking into account electronic degrees of freedom. The proton momentum distribution analysis based on Gram–Charlier expansion gives, in addition to the widths of momentum distribution, small but clearly visible non-harmonic effects in both ammonium salts: the values of kurtosis of momentum distribution are non-vanishing but do not increase or decrease systematically with increasing scattering angle (decreasing scattering time). The values are identical within statistical accuracy of the analysis and equal to 0.02. Non-vanishing kurtosis is responsible for a shift of the proton momentum distribution to higher momentum values. Values of kurtosis around 0.2 have already been obtained for supercritical [7] and pure water [9]. Slightly higher values, approx. 0.3, have been obtained for ice I_h and ice VI [8]. In both cases a shift in proton momentum distribution was interpreted to be the result of binding of the proton to its covalently bonded atom. The reported NCS results from both systems seem to give evidence that this is also the case for a proton covalently bonded to the nitrogen atom in the NH_4^+ molecule. The proton momentum distribution can be thought of as arising from its confinement in the potential well provided by the nitrogen atoms, which can be regarded as fixed in position in the timescale of proton motion. Thus, the effect of nitrogen atoms on the proton's momentum distribution cannot be really thought of as arising from a static potential. The nitrogen atoms in NH_4^+ provide thus a single-particle effective potential [7]. For the values of kurtosis of proton momentum distribution below 0.3 the inversion procedure of the momentum distribution function leads to a single-well potential, in contrast to kurtosis values above 0.3 leading to double-well potentials where protons are tunneling [7, 9, 8, 10].

The anomaly of the proton scattering intensities is almost identical for all scattering angles between 30° and 60° when the measured proton momentum distribution is fitted by Gaussian and non-Gaussian Compton profiles. In both $(NH_4)_2PdCl_6$ and $(NH_4)_2TeCl_6$ the anomaly of the proton scattering intensity reaches its maximum at scattering angles between 50° and 60°; then it starts decreasing with decreasing scattering angle to cease at the scattering angle of about 30°. Moreover, a very good agreement has been obtained using two independent data treatment schemes: a model-free Dorner method [26, 48, 50] and the center-of-peak method [27]. This supports the hypothesis, put forward in a previous NCS study of ammonium hexachloropalladate and ammonium hexachlorotellurate, that the anomaly may disappear at the timescale of the order of approx. 1 fs due to the coupling of proton and environment degrees of freedom [32]. The constancy of the standard deviation of proton momentum distribution on the one side and the angular dependence of the anomaly of neutron scattering cross section of protons in ammonium hexachloropalladate and hexachlorotellurate on the other side lead to the conclusion that there is no extra broadening or peak shift of proton momentum distribution due to ultra-fast kinetics of Compton scattering in both systems. This experimental result has important consequences for theoretical models attempting to explain the anomaly in terms of non-Born–Oppenheimer proton dynamics in the final state of the NCS scattering process [34–36].

The theory by Reiter and Platzman [35] predicts that, in the strong coupling region, the proton NCS recoil peak is shifted to lower energies [35]. Also, in the model by Gidopoulos [34] a broadening of momentum distribution is expected if one goes beyond the simplest case of a two-level electronic system accessed by the proton in the final

state of the collision. In simple terms, the predicted proton momentum distribution would then consist of a distribution of peaks shifted from the center of the main recoil line by different amounts of energy corresponding to a proton accessing different excited electronic levels in the final state. From the data treatment point of view the broadening resulting from both theories would manifest itself in three possible ways: (i) increase of the width of the proton momentum distribution with increasing scattering angle, (ii) increase of the non-harmonic contribution to the proton recoil lineshape with increasing scattering angle and/or (iii) as a broad slowly varying background in TOF. The contributions of type (i) and type (ii) have not been detected as there is no visible trend in the values of kurtosis of momentum distributions in both systems as a function of the scattering angle. The contribution of type (ii) cannot be entirely excluded as all forward scattering spectra recorded did contain some broad background that was accounted for by fitting third-order polynomial functions in TOF. Ideally, such a broad background would persist for all forward scattering angles. Unfortunately, the TOF background on VESUVIO changes from detector to detector, which makes the assessment about any systematic contributions impossible.

In light of the results of the proton momentum distribution analysis presented above the predictions of models seem especially interesting where electronic degrees of freedom are either not involved at all in the description of anomalous scattering or they couple weakly to nuclear degrees of freedom. The first situation is present in the model by Karlsson and Lovesey [37–39]. In their model the spatial form of the scattering function is not modified by the presence of the exchange coupling. The reduced scattering intensities arise solely from the factors multiplying the scattering function [39]. This theoretical result has a very important consequence: the observed deficit of the scattering intensity can be explained without resorting to breaking the first moment sum rule [39].

The second situation is encountered in the model put forward by Mazets *et al* [36]. In their model of ultra-fast scattering process a neutron impinges on a projectile composed of the nucleus of interest and electrons being coupled to environmental electronic degrees of freedom with the coupling strength given by a momentum-transfer-dependent relaxation rate [36]. The inclusion of fast environmentally induced relaxation in the theoretical description of the neutron Compton scattering leads to a generalized (skewed) Lorentzian lineshape of the final (target and projectile) state induced by the environment. If the spread of the nuclear momentum distribution in the initial state of the target nucleus is much larger than that of the lineshape of the final state only the anomaly of the scattering intensity of target nuclei without any extra broadening is observed. However, if the experimental data require that the magnitude of the anomaly be large, a very large relaxation rate is needed. In such a case the theory predicts an extra broadening of the experimental lineshape beyond that of the initial-state momentum distribution of the target nucleus [36]. If the model by Kurizki *et al* still applies in the case of NCS scattering on ammonium hexachloropalladate and ammonium hexachlorotellurate the fact that no extra broadening is observed, even for values of momentum and energy transfers for which the largest magnitude of the anomaly is observed, would have to imply that the coupling between the relevant electronic degrees of freedom of the target (ammonium ion protons) and the environment is in the weak or intermediate regime in the entire energy transfer domain accessible (from 3 eV at the scattering angle of 30° up to 40 eV at the scattering angle of 70°).

The theory by Chatzidimitriou-Dreismann [14, 2], based on attosecond quantum dynamics and decoherence in *open quantum systems*, leads to a considerably more complicated interrelation between H-momentum distribution and anomalous intensity (work in progress). This relation is of intrinsic character and depends on specific details of the local electronic environment (in short: potential) of the struck proton, which then may lead to various degrees of decoherence. The latter contributes to both the H-intensity and H-momentum distribution. For example, in an asymmetric three-dimensional potential, the decoherence channels (and/or mechanisms) are predicted to be quantitatively different in the q directions of a 'weak' (or flat) and 'strong' (or steep) local potential. In very illustrative terms: for a weak potential along q, the struck proton will 'explore' a *larger* spatial regime during its scattering time [21], which then implies *enhanced* decoherence; and vice versa for the case of a strong potential along q. According to [14, 2], this difference is expected to depend on q too. Obviously, this physical mechanism strongly contradicts a claim of [3], according to which there is no physical relation between the physical quantities 'H-intensity deficit' and 'momentum distribution'. However, in the case of the two systems studied in this paper, the local potential of a proton is highly symmetric, and thus the aforementioned interrelationship should be masked by this.

9. Conclusions

In both ammonium hexachloropalladate and ammonium hexachlorotellurate, the reduction factor of the neutron scattering intensity of protons was found to be smaller than unity, thus indicating the anomalous neutron Compton scattering. The largest magnitude of the anomaly is found for both systems at scattering angles between 50° and 60°, being approx. 20%. Interestingly, the anomaly decreases with decreasing scattering angle and disappears in both systems at the scattering angle of approx. 30°. The dependence of the magnitude of the anomaly on the scattering angle is the same in both substances within experimental error. A new NCS 'center-of-peak' data treatment scheme and the method proposed by Dorner were applied for the first time for the case of time-of-flight spectra consisting of more than two recoil peaks. The values of the reduction factor calculated using the 'center-of-peak' and Dorner methods are in very good agreement with the values calculated from the standard CA approach.

In contrast to the scattering intensities, no systematic broadening or peak shift of proton momentum distributions with increasing scattering angle (decreasing scattering time) was observed in $(NH_4)_2PdCl_6$ and $(NH_4)_2TeCl_6$. The widths obtained by fitting both a Gaussian and the usually applied form of the Gram–Charlier expansion [3, 4] to measured proton

momentum distributions are, within experimental accuracy, equal to 5.0 $Å^{-1}$ in both $(NH_4)_2PdCl_6$ and $(NH_4)_2TeCl_6$. This result is in very good agreement with values calculated for isolated ammonium ion (decoupled from the dynamics of the sublattice of the octahedral anions $PdCl_6^{2-}$ and $TeCl_6^{2-}$) using a semiclassical *ab initio* approach including vibrational, translational and rotational contributions to the mean kinetic energy. The fact that the deficit of the scattering intensity of protons is independent of the proton momentum distribution is most probably due to the highly symmetric local effective potential the protons experience in both systems. This observation has far-reaching consequences for further theoretical work on the role of electronic degrees of freedom in the anomaly of the scattering intensity as observed by neutron Compton scattering.

Acknowledgment

Financial support from the Deutsche Forschungsgemeinschaft (grant no. KR 3489/1–1) program is acknowledged.

References

[1] Watson G I 1996 *J. Phys.: Condens. Matter* **8** 5955
[2] Chatzidimitriou-Dreismann C A 2005 *Laser Phys.* **15** 780
[3] Andreani C, Colognesi D, Mayers J, Reiter G F and Senesi R 2005 *Adv. Phys.* **55** 377
[4] Garbuio V, Andreani C, Imberti S, Pietropaolo A, Reiter G F, Senesi R and Ricci M A 2007 *J. Chem. Phys.* **127** 154501
[5] Krzystyniak M and Chatzidimitriou-Dreismann C A 2009 in preparation
[6] Glyde H R 1996 *Phys. Rev.* B **50** 6726
[7] Reiter G F, Li J C, Mayers J, Abdul-Redah T and Platzman P 2004 *Braz. J. Phys.* **34** 142
[8] Reiter G F, Burhham C, Homouz D, Platzman P M, Mayers J, Abdul-Redah T, Morawsky A P, Li J C, Loong C-K and Kolesnikov A I 2006 *Phys. Rev. Lett.* **97** 247801
[9] Reiter G F, Mayers J and Abdul-Redah T 2006 *Physica* B **385/386** 234
[10] Reiter G F, Mayers J and Noreland J 2002 *Phys. Rev.* B **65** 104305
[11] Chatzidimitriou-Dreismann C A, Abdul-Redah T, Streffer R M F and Mayers J 1997 *Phys. Rev. Lett.* **79** 2839
[12] Karlsson E B, Abdul-Redah T, Streffer R M F, Hjörvarsson B, Mayers J and Chatzidimitriou-Dreismann C A 2003 *Phys. Rev.* B **67** 184108
[13] Abdul-Redah T and Chatzidimitriou-Dreismann C A 2004 *Physica* B **350** e1035
[14] Chatzidimitriou-Dreismann C A, Abdul-Redah T and Sperling J 2000 *J. Chem. Phys.* **113** 2784
[15] Chatzidimitriou-Dreismann C A, Abdul-Redah T, Streffer R M F and Mayers J 2002 *J. Chem. Phys.* **116** 1511
[16] Chatzidimitriou-Dreismann C A, Abdul-Redah T and Kolaric B 2001 *J. Am. Chem. Soc.* **123** 11945
[17] Karlsson E B, Chatzidimitriou-Dreismann C A, Abdul Redah T, Streffer R M F, Hjörvarsson B, Öhrmalm J and Mayers J 1999 *Europhys. Lett.* **46** 617
[18] Chatzidimitriou-Dreismann C A, Vos M, Kleiner C and Abdul-Redah T 2003 *Phys. Rev. Lett.* **91** 057403
[19] Cooper G, Hitchcock A P and Chatzidimitriou-Dreismann C A 2008 *Phys. Rev. Lett.* **100** 043204
[20] Mayers J and Abdul-Redah T 2004 *J. Phys.: Condens. Matter* **16** 4811
[21] Sears V F 1984 *Phys. Rev.* B **30** 44
[22] Blostein J J, Dawidowski J and Granada J R 2001 *Physica* B **304** 357
[23] Blostein J J, Dawidowski J and Granada J R 2003 *Physica* B **334** 257
[24] Blostein J J, Dawidowski J and Granada J R 2004 *Nucl. Instrum. Methods* B **217** 333
[25] Blostein J J, Dawidowski J and Granada J R 2005 *Phys. Rev.* B **71** 054105
[26] Dorner B 2005 *J. Neutron Res.* **13** 267
[27] Krzystyniak M and Chatzidimitriou-Dreismann C A 2008 *J. Phys.: Condens. Matter* **20** 104249
[28] Birczynski A, Lalowicz Z T and Lodziana Z 2004 *Chem. Phys.* **299** 113
[29] Lalowicz Z T, McDowell C A and Raghunathan P 1979 *J. Chem. Phys.* **70** 4819
[30] Olejniczak Z *et al* 2002 *J. Chem. Phys.* **116** 10343
[31] Birczynski A, Lalowicz Z T and Lodziana Z 2001 *Mol. Phys. Rep.* **31** 117
[32] Krzystyniak M, Chatzidimitriou-Dreismann C A, Lerch M, Lalowicz Z T and Szymocha A 2007 *J. Chem. Phys.* **126** 124501
[33] Gupta B R K, Kawald U, Johannsmann H, Pellit J and Xu Y C 1992 *J. Phys.: Condens. Matter* **4** 6879
[34] Gidopoulos N 2005 *Phys. Rev.* B **71** 054106
[35] Reiter G F and Platzman P M 2005 *Phys. Rev.* B **71** 054107
[36] Mazets I E, Chatzidimitriou-Dreismann C A and Kurizki G 2005 *Decoherence, Entanglement and Information Protection in Complex Quantum Systems* ed V M Akulin *et al* (Dordrecht: Springer) p 549
[37] Karlsson E B and Lovesey S W 2000 *Phys. Rev.* A **61** 062714
[38] Karlsson E B and Lovesey S W 2002 *Phys. Scr.* **65** 112
[39] Karlsson E B 2008 *Phys. Scr.* **77** 065301
[40] Mayers J, Andreani C and Baciocco G 1989 *Phys. Rev.* B **39** 2022
[41] Mayers J 1990 *Phys. Rev.* B **41** 41
[42] Mayers J 1993 *Phys. Rev. Lett.* **71** 1553
[43] Andreani C, Colognesi D and Pace E 1999 *Phys. Rev.* B **60** 10008
[44] West G B 1975 *Phys. Rep.* C **18** 263
[45] Evans A C, Timms D N, Mayers J and Bennington S M 1996 *Phys. Rev.* B **53** 3023
[46] Lovesey S W 1984 *Theory of Neutron Scattering from Condensed Matter* (Oxford: Clarendon)
[47] Cowley R A 2003 *J. Phys.: Condens. Matter* **15** 4143
[48] Dorner B 2006 *Nucl. Instrum. Methods* B **247** 390
[49] Krzystyniak M and Chatzidimitriou-Dreismann C A 2006 *J. Neutron Res.* **14** 193
[50] Krzystyniak M and Chatzidimitriou-Dreismann C A 2005 *Phys. Rev.* B **72** 174117
[51] Colognesi D *et al* 2001 *Physica* B **293** 317
[52] Andreani C *et al* 2001 *J. Chem. Phys.* **114** 387
[53] Mitchell P C H, Parker S F, Ramirez-Cuesta A J and Tomkinson J 2005 *Vibrational Spectroscopy with Neutrons* (Singapore: World Scientific)
[54] Andersson M P and Uvdal P 2005 *J. Phys. Chem.* A **109** 2937
[55] Nakamoto K 1997 *Infrared and Raman Spectra of Inorganic and Coordination Compounds* (New York: Wiley)
[56] Becke A D 1993 *J. Chem. Phys.* **98** 1372
[57] Scott A P and Radom L J 1996 *Phys. Chem.* **100** 16502
[58] Ramirez-Cuesta A J 2004 *Comput. Phys. Commun.* **157** 226
[59] Bright Wilson E, Decius J C and Cross P C 1980 *Molecular Vibrations, the Theory of Infrared and Raman Vibrational Spectra* (New York: Dover)
[60] Ochterski J W 1999 *Vibrational Analysis in Gaussian* http://www.gaussian.com/g_whitepap/vib.htm